seawater (Fig. 2), according to the following relationship.

$$\mathrm{DIP}\ (\mu\mathrm{mol/L}) = 1.43\ (\pm 0.07) \times \mathrm{P/Ca}\ (\mathrm{mmol/mol}) + 0.13\ (\pm 0.05) \quad (1)$$
$$r^2 = 0.99, P = 0.0001$$

Errors on the regression are calculated with respect to the dispersion on the *y* axis and are given at 1 SE.

To test the robustness of the phosphorus calibration based on modern global data sets, Eq. 1 was applied to long-lived modern specimens (COBAS 97a and COBAS 98) from the western Mediterranean Sea, with growth encompassing about the past 30 years. Both coral samples show an increase in P/Ca ratio of ~1.2% per year over this period (Fig. 3), in agreement with direct measurements of nutrients, reflecting the effects of increasing agricultural, industrial, and urban activities in the Mediterranean countries since the 1960s (*29*). In addition to the general positive trend in the nutrient content for the past 30 years, P content within *D. dianthus* also reveals decadal-scale variations within the water column and an almost constant offset between the two specimens over the growth period, suggesting a connected evolution at different water depths.

To further demonstrate the utility of this new proxy, we have examined premodern and fossil *D. dianthus* samples dredged from submerged coral assemblages in the western Mediterranean Sea. The most striking feature of these samples, which have ages within ~120 to ~11,190 years before the present (yr B.P.) (^{230}Th-^{238}U ages) (table S1), is their high P/Ca ratios (Fig. 3), which indicate the presence of more nutrient-rich deep waters. In particular the P content of the submodern coral COBAS 97c is almost twice that of present-day values, with even higher levels being found in a 11,230-year-old coral (LM 99-124), indicating nutrient-rich seawater similar to the present-day Chilean eutrophic environment.

These results are also consistent with phytoliths and freshwater diatom records from sediment cores in the western Mediterranean Sea, which suggest the establishment of humid conditions at the end of the Younger Dryas event, related to an intensification of the African monsoon (*30*). This might have led to an increase of phosphate availability, which in the Mediterranean is mainly related to river runoff (*29*). These results confirm the utility of cold-water coral *D. dianthus* as a proxy for seawater P, providing a new tool for reconstructing changes in the nutrient status of the oceans.

References and Notes

1. C. R. Benitez-Nelson, *Earth Sci. Rev.* **51**, 109 (2000).
2. T. Tyrrell, *Nature* **400**, 525 (1999).
3. M. L. Delaney, *Global Biogeochem. Cycles* **12**, 563 (1998).
4. D. M. Sigman, E. A. Boyle, *Nature* **407**, 859 (2000).
5. H. J. Spero, J. Bijma, D. W. Lea, B. E. Bemis, *Nature* **390**, 497 (1997).
6. R. E. M. Rickaby, H. Elderfield, *Paleoceanography* **14**, 293 (1999).
7. T. M. Marchitto, *Geochem. Geophys. Geosyst.* **5**, Q10D11 (2004).
8. J. Dymond, E. Suess, M. Lyle, *Paleoceanography* **7**, 163 (1992).
9. P. Bertrand, E. Lallier-Vergès, *Nature* **364**, 786 (1993).
10. J. McManus *et al.*, *Geochim. Cosmochim. Acta* **62**, 3453 (1998).
11. S. G. Wakeham, C. Lee, in *Organic Geochemistry*, M. Engel, S. Macko, Eds. (Plenum, New York, 1993), pp. 145–169.
12. R. E. Dodge, T. D. Jickells, A. H. Knap, S. Boyd, R. P. M. Bak, *Mar. Pollut. Bull.* **15**, 178 (1984).
13. W. Shotyk, I. Immenhauser-Potthast, H. A. Vogel, *J. Chromatogr.* **706**, 209 (1995).
14. C. E. Rasmussen, C. Cuff, *Proc. Fourth Pacific Congress on Marine Science and Technology* **1**, 13 (1990).
15. J. F. Adkins, H. Cheng, E. A. Boyle, E. R. M. Druffel, R. L. Edwards, *Science* **280**, 725 (1998).
16. J. M. Heikoop, D. D. Hickmott, M. J. Risk, C. K. Shearer, V. Atudorei, *Hydrobiologia* **471**, 117 (2002).
17. O. A. Sherwood *et al.*, *Mar. Ecol. Prog. Ser.* **301**, 135 (2005).
18. S. D. Cairns, G. D. Stanley Jr., *Proc. Fourth Internatl. Coral Reef Symposium* **1**, 611 (1981).
19. G. Försterra, V. Häussermann, *Zool. Verth. Leiden* **345**, 117 (2003).
20. Materials and methods are available as supporting material on *Science* Online.
21. F. Norambuena, thesis, Universidad Austral de Chile (2002).
22. M. McCulloch *et al.*, *Program and Abstract Book of the Third Internatl. Symposium on Deep-Sea Corals*, Miami 191 (2005).
23. H. Cheng, J. Adkins, R. L. Edwards, E. A. Boyle, *Geochim. Cosmochim. Acta* **64**, 2401 (2000).
24. P. Montagna, M. T. McCulloch, M. Taviani, A. Remia, C. Mazzoli, *Program and Abstract Book of the Third Internatl. Symposium on Deep-Sea Corals*, Miami 193 (2005).
25. P. Montagna, M. T. McCulloch, T. Taviani, A. Remia, G. Rouse, in *Cold-Water Corals and Ecosystems*, A. Freiwald, J. M. Roberts, Eds. (Springer-Verlag, Berlin, Heidelberg, 2005), pp. 671–688.
26. C. Alibert *et al.*, *Geochim. Cosmochim. Acta* **67**, 231 (2003).
27. Y. L. Addadi, S. Raz, S. Weiner, *Adv. Mater.* **15**, 959 (2003).
28. J. Stolarski, *Acta Palaeontol. Pol.* **48**, 497 (2003).
29. J. P. Béthoux *et al.*, *Mar. Chem.* **63**, 155 (1998).
30. M. A. Bárcena *et al.*, *Palaeogeogr. Palaeoclimatol. Palaeoecol.* **167**, 337 (2001).

31. We thank G. Mortimer and L. Kinsley for U-series dating and technical assistance with laser ablation analysis, respectively. We are grateful to S. Castelli for technical photographic support, S. Frisia and M. Prieto for suggestions on the P incorporation into aragonite, and S. Russo for helping on the moving correlation analysis. We are also grateful to C. Ianni, V. Brando, and J. Sepulveda for helping in the acquisition of the DIP data from the Ionian Sea, the Australian sector of the western Pacific Ocean, and the Chilean fjords, respectively; G. Forsterra for sampling the Chilean corals; and the Australian Museum for access to their collections. The work by P.M. was supported by a Ph.D. scholarship of the University of Padova and by the Ermenegildo Zegna Foundation. Support from the Australian Research Council Centre of Excellence for Coral Reef Studies and grant DP0559042 to M.Mc. is gratefully acknowledged, as well as partial funding to M.T. by European Science Foundation Moundforce and European Union Hermes programs and Ismar-Bologna contribution 1506.

Supporting Online Material

www.sciencemag.org/cgi/content/full/312/5781/1788/DC1
Materials and Methods
SOM Text
Figs. S1 to S4
Table S1
References

3 February 2006; accepted 11 May 2006
10.1126/science.1125781

The Structure of an Infectious P22 Virion Shows the Signal for Headful DNA Packaging

Gabriel C. Lander,[1,2] Liang Tang,[1] Sherwood R. Casjens,[3] Eddie B. Gilcrease,[3] Peter Prevelige,[4] Anton Poliakov,[4] Clinton S. Potter,[2] Bridget Carragher,[2] John E. Johnson[1]*

Bacteriophages, herpesviruses, and other large double-stranded DNA (dsDNA) viruses contain molecular machines that pump DNA into preassembled procapsids, generating internal capsid pressures exceeding, by 10-fold, that of bottled champagne. A 17 angstrom resolution asymmetric reconstruction of the infectious P22 virion reveals that tightly spooled DNA about the portal dodecamer forces a conformation that is significantly different from that observed in isolated portals assembled from ectopically expressed protein. We propose that the tight dsDNA spooling activates the switch that signals the headful chromosome packing density to the particle exterior.

Since its discovery in 1952, the bacteriophage P22, which infects *Salmonella enterica*, has been an intensely studied model for virus assembly (*1*, *2*). The assembly pathway of P22, illustrating the role of the portal protein (gp1) as a conduit for DNA packaging, is shown in Fig. 1. As in many other dsDNA viruses, a sensor that detects chromosome density within the capsid independently of DNA sequence controls termination of genome packaging. Genetic studies showed that the portal plays this role, but how events occurring within the particle are detected and signaled to exterior packaging machinery remains unclear. Here we show a three-dimensional reconstruction of infectious P22 particles determined without applying icosahedral symmetry, revealing the portal switch in an activated state, presumably triggered by close contact with spooled dsDNA. Comparison of this structure with the previously determined free portal

structure indicates a large-scale reorganization of the portal, which can explain the signal transduction pathway from inside to outside of the particle.

The validation of the asymmetric reconstruction depends on previous studies in which several components of the P22 virion machinery were isolated and their structures determined by x-ray crystallography or cryo–electron microscopy (cryo-EM). The crystal structure of the gp9 tail spike (an endorhamnosidase that binds to and cuts the O-antigen polysaccharide receptor on the bacteria) was solved as two separate fragments, the virion-binding domain (residues 1 to 124) at 2.3 Å resolution and the receptor-binding domain (residues 109 to 666) at 1.6 Å (*3*, *4*). Cryo-EM was used to determine the structure of the entire tail machine structure (gp1, 4, 9, 10, and 26), isolated from virions, at 25 Å (*5*). P22 coat protein shell structures before and after expansion were determined at subnanometer resolution by cryo-EM and icosahedral averaging (*6*). Such averaging ignores the fact that one pentameric vertex is occupied by the portal ring in the procapsid and the whole tail machine in the virion. At this resolution some secondary structural elements of the coat protein subunit and conformational changes undergone during capsid expansion were observed, but icosahedral averaging eliminates the density for any non-icosahedral structural features. Cryo-EM reconstructions of bacteriophages T7 (*7*, *8*), T4 (*9*), and ϕ29 (*10*–*12*) have been determined without icosahedral averaging (asymmetric reconstructions) and supplied qualitative insight into the organization of these capsids; however, these lower-resolution reconstructions did not reveal details of the packaging machinery. Recently the structure of phage epsilon 15 was determined as an asymmetric reconstruction (*13*), with packaged DNA and details of the portal visible as well. However, crystal structures are not available for any of the viral components, nor is there any genetic or biochemical information about the function or location of gene products.

The asymmetric reconstruction of the P22 virion electron density exhibited the expected $T = 7l$ coat protein lattice (a left-handed lattice containing seven subunits in an icosahedral asymetric unit) observed in the icosahedrally averaged reconstruction, with a hexameric tail assembly replacing one pentamer vertex (Fig. 2). The color-coded location of the P22 gene products in the particle is shown in Fig. 3A. The portal can be readily identified within the interior of the capsid by its 12-fold symmetry (Fig. 3, B and C). The overall organization of the viral tail machine was in excellent agreement with the earlier reconstruction of the isolated tail complex (*5*). Furthermore, the virion density of the individual tail spike gp9 trimers envelopes the x-ray model (*3*) of the receptor-binding portion of gp9 with exceptional accuracy (Fig. 4A). Attachment of gp9 to the tail-machine tube occurs in two places on each tail-spike trimer, which suggests that it interacts with both gp4 and gp10. The close similarities of the coat protein lattice, the tail machine, and the isolated tail-spike portions of the asymmetric reconstruction of the P22 virion to independently determined substructures indicate that the reconstruction strategy accurately reproduces the native structure of the virion [see supporting online material (SOM)].

All tailed phages have a symmetry mismatch between the tail machine's 12-fold symmetric portal and a 5-fold axis of the coat protein shell (Fig. 4B). Such a mismatch has been postulated to facilitate rotational movements during the packaging of DNA (*14*–*16*). Although this reconstruction neither proves nor disproves the possibility of portal rotation upon DNA packaging, the precision of the tail machine density in the reconstruction requires that it must always be aligned in a particular spatial orientation with respect to the pentavalent coat lattice opening. Thus, the portal in the infectious particle must always occupy one of five equivalent registers within the capsid opening.

Ectopically expressed gp1 assembles into ringlike structures in vitro (*5*). The plasmid expressed protein used for crystallography (102 amino acids were removed from its C terminus to increase its solubility in vitro) was analyzed by cryo-EM, and two populations of rings were identified, ~80% with 11-fold symmetry and 20% with 12-fold symmetry. These populations could be computationally segregated, and the highest-resolution reconstruction was obtained of the 11-fold portal structure. Comparison of this

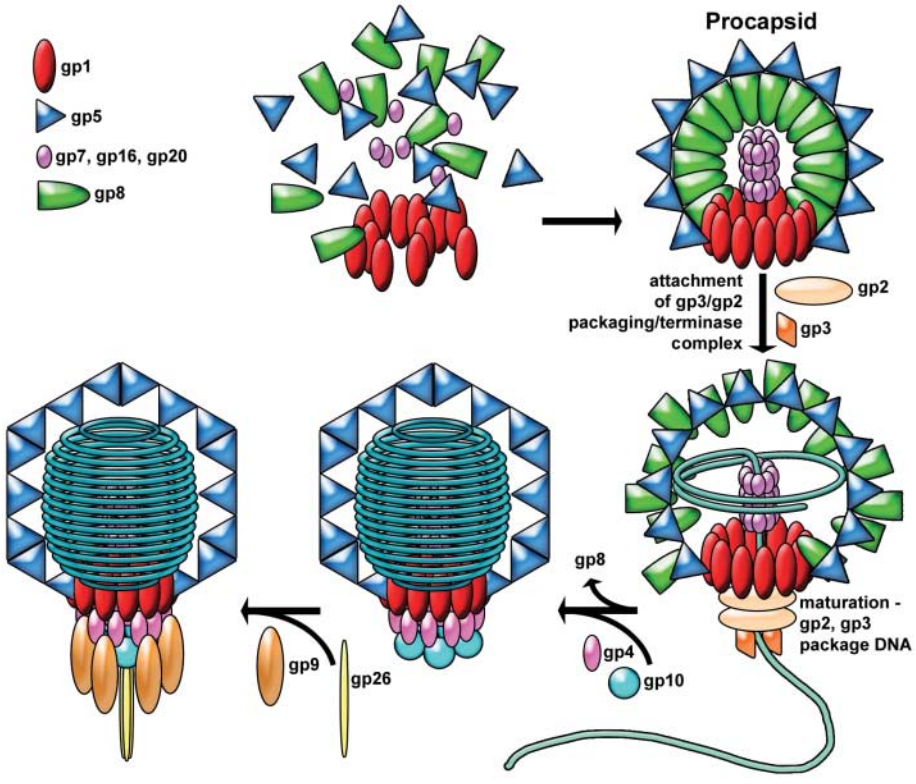

Fig. 1. The bacteriophage P22 assembly pathway. P22 assembles a protein precursor particle called a procapsid, which is the receptacle into which its 43.5 thousand base pairs (kbp) DNA chromosome is packaged. P22 procapsid shells are built from two major components, 415 molecules of coat protein (gp5, the product of gene *5*) arranged in a $T = 7l$ icosahedral shell and roughly 250 molecules of scaffolding protein (gp8) within the coat protein shell. In addition, smaller numbers of four other proteins are present in the procapsid. A dodecamer of 84-kD proteins (gp1) is present at a single unique icosahedral vertex. Six to 20 intravirion molecules of the products of genes *7*, *16*, and *20* are required for successful DNA injection into susceptible cells and are released from the virion during the injection process. As DNA is packaged, the thick procapsid shell expands from a radius of about 55 nm to a thinner, more angular shell 65 nm in diameter. Despite having a genome 41.7 kbp in length, P22 packages DNA until the capacity of the capsid is reached, ~43.5 kbp, a strategy referred to as "headful" DNA packaging. Termination of packaging by cleavage of the concatemeric DNA is initiated not by sequence, but when the chromosome is at a defined packing density that is sensed by portal protein. After DNA is packaged, the tail assembly is constructed by the sequential addition of multiple copies of four gene products (gp4, gp10, gp26, and gp9) to the vertex occupied by the portal ring [for further details see references (*1*, *2*, *5*) and references therein].

[1]Department of Molecular Biology, The Scripps Research Institute, 10550 North Torrey Pines Road, La Jolla, CA 92037, USA. [2]National Resource for Automated Molecular Microscopy, Department of Cell Biology, The Scripps Research Institute, 10550 North Torrey Pines Road, La Jolla, CA 92037, USA. [3]Department of Pathology, University of Utah School of Medicine, Salt Lake City, UT 84112, USA. [4]Department of Microbiology, University of Alabama at Birmingham, Birmingham, AL 35294, USA.

*To whom correspondence should be addressed. E-mail: jackj@scripps.edu

structure of the isolated P22 portal with the portal in the virion reconstruction revealed a significant reorganization during assembly and maturation of the virion (Fig. 4C). Part of this apparent change in conformation may be due to the missing 102 amino acids at the C terminus of the isolated protein; however, the extensive differences between the two structures imply that portions of the portal adopt a different conformation in the virion than when it is isolated in solution.

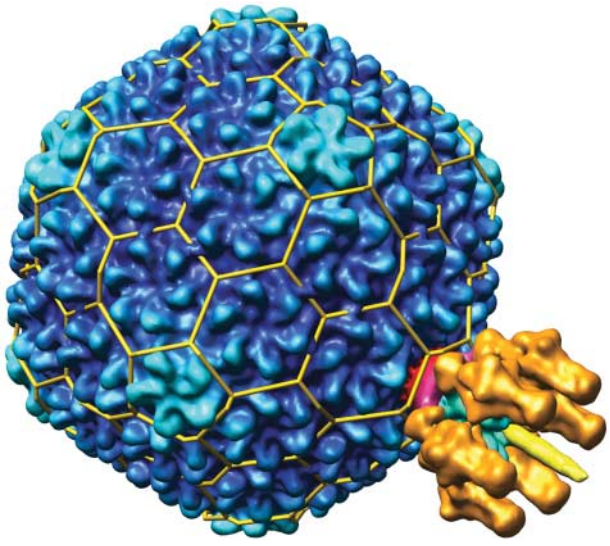

Fig. 2. Surface volume representation of the P22 bacteriophage infectious virion at 17 Å resolution. A three-dimensional reconstruction of the P22 virion resulting from the superposition of 26442 particles is shown with the same coloring scheme as in Fig. 1. The $T = 7l$ organization (indicated by the yellow lattice cage) of the coat proteins (blue) is clearly visible in the reconstruction without the imposition of icosahedral symmetry. The tail machinery, which exhibits 6- and 12-fold symmetry at different distances from the virion center, is situated at a single five-fold vertex of the capsid and replaces five coat subunits there.

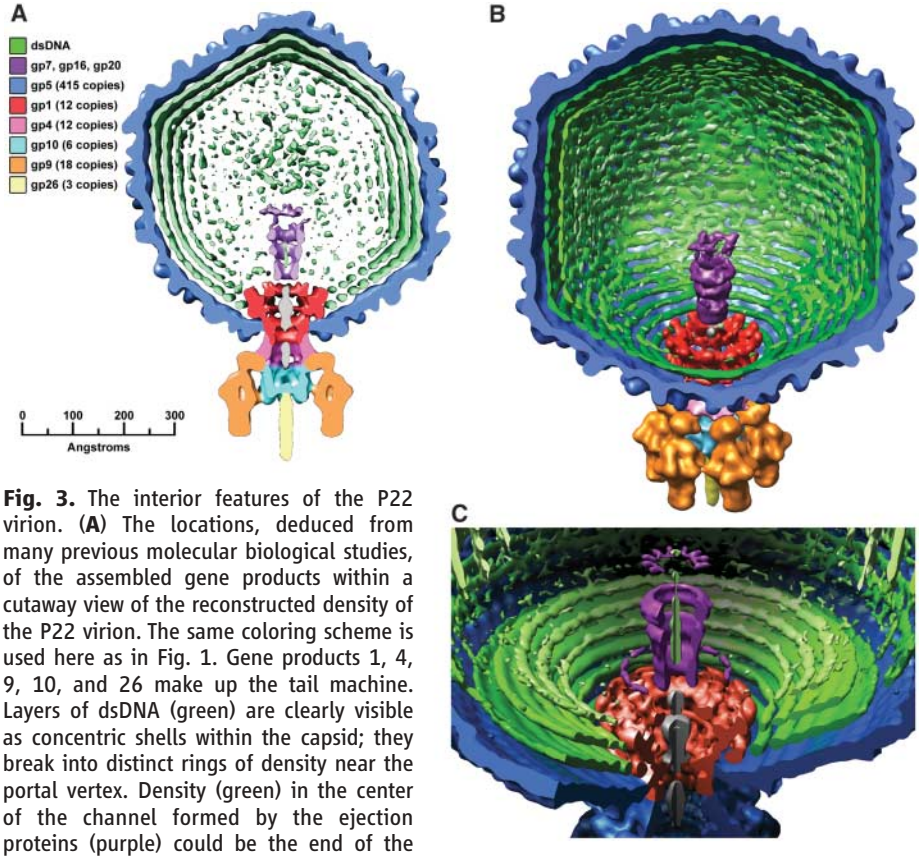

Fig. 3. The interior features of the P22 virion. (**A**) The locations, deduced from many previous molecular biological studies, of the assembled gene products within a cutaway view of the reconstructed density of the P22 virion. The same coloring scheme is used here as in Fig. 1. Gene products 1, 4, 9, 10, and 26 make up the tail machine. Layers of dsDNA (green) are clearly visible as concentric shells within the capsid; they break into distinct rings of density near the portal vertex. Density (green) in the center of the channel formed by the ejection proteins (purple) could be the end of the P22 chromosome; however, density on this axis within the portal protein ring (red) does not appear to be consistent with DNA. (**B**) A cutaway view of the internal portion of the asymmetrically reconstructed particle contoured at 3 σ, showing the 12-fold symmetry of the portal (red), the putative ejection proteins (purple), and individual strands of dsDNA (green). (**C**) Close-up view of the packaged interior upon 12-fold averaging along the tail tube axis. Although the E-proteins (purple) themselves in reality may or may not exhibit 12-fold symmetry, this view demonstrates the channel-like nature of the structure they form in the virion, as well as the dsDNA (green) that may be seated within their channel. Three concentric shells of spooled DNA are clearly visible.

Termination of DNA packaging when the P22 head is full implies a pressure sensor that conveys a signal from within the particle to the exterior, which initiates a program of cutting the DNA (by the gp2/gp3 terminase complex), release of gp2 and gp3, and attachment of the other components of the tail machine (gp4, 10, 9, and 26) to the portal (Fig. 1). The reconstruction shows that the portal ring extends from the capsid interior (where it makes direct contact with packaged DNA) to the outside (where it must make direct contact with the DNA gp2/gp3 packaging-terminase complex, during the DNA filling process). The structural change of the portal from a "low-pressure" free state to a "high-pressure" assembled state is consistent with the portal as the signal transducer of a full head of DNA. Indeed, Casjens *et al*. (*17*) proposed a role for the portal in headful sensing when they found that two different single–amino acid changes (near the N terminus and the middle of the protein) each caused 2000 extra base pairs to be encapsidated before the packaged DNA was cleaved from the remaining concatemeric DNA. Examination of the intravirion portal shows a tightly wound ring of dsDNA (resulting from averaging many particles with different start points for the duplex spiral into the next ring) surrounding a region of the portal that has undergone a conformational change (Fig. 4C) relative to the free form. We suggest, therefore, that the portal is in the isolated form within the procapsid as packaging of the DNA commences. As the DNA continues to enter and is spooled into the capsid, the resulting increase in pressure forces DNA to tighten around the portal. At a critical point in the packaging process, when the capsid has fully expanded and with the chromosome at the headful density, the surrounding ring of DNA exerts such a force on the portal that it changes conformation, signaling the packaging motor to cease and the packaging-terminase complex to cut the packaged chromosome from the remaining concatemeric DNA. The new portal conformation can bind the remaining gene products that form the tail machinery required for infection. Although it was not discussed in detail, a similar ring of apparent DNA density was seen in the asymmetric reconstructions of T7 and epsilon 15 virions (*7*, *13*), suggesting that such a portal-DNA interaction may be a general feature of the tailed-phage virions.

Further support for this hypothesis is evidenced by a comparison of the P22 portal to the crystal structure of the phage ϕ29 portal. Although it does not use the headful packaging mechanism, ϕ29 uses a DNA translocase that is similar to other tailed phages (*18*). Docking of the ϕ29 portal crystal structure (*15*) into the P22 portal density reveals an exceptionally good fit to the lower stalk region that extends outside of the particle and to the lower portion of the wing region that makes contact with the capsid protein. However,

the model of P22 does not extend to the density that is in the upper part of the wing and above the wing in the high-pressure form (fig. S4). This comparison suggests that the additional 416 residues per subunit in the P22 portal are required for pressure sensing, while a structural core of similar size to the ϕ29 portal (307 residues) participates in DNA packaging.

In addition to the tail machine and packaging proteins discussed above, multiple molecules of the products of genes *7*, *16*, and *20* are also present in the infectious virion (*19*). They are not essential for assembly of virion-like particles that contain DNA (*19*–*21*), but are ejected from the virion during DNA injection (*22*) and are required for successful DNA injection into the host cell (*20*, *23*). One or more of these ejection proteins are likely to form the tubular set of electron densities above the portal and around the central axis of the tail machine. This density is not dsDNA (Fig. 3B), because of its size and morphology, as well as the fact that the inner channel is occupied with density that is probably dsDNA aligned with the tail-machine tube. Another candidate for an ejection protein is density within the portal and tail machine that is clearly not dsDNA, but rather a plug-like density (colored gray in Fig. 3C) that probably aids in maintaining the highly pressurized DNA within the capsid.

The virion structure reported here is valuable for understanding the P22 assembly program as well as the mechanism of injection of DNA into susceptible cells. All of the major components of P22 were recognized in the reconstruction (Fig. 3A), and candidates for minor components were identified, and DNA is clearly recognizable in the particle's interior. There are no proteins in tailed-phage virions that hold the DNA in place (*14*), so the internal rings of density must be the packaged DNA. The observed dsDNA density is consistent with DNA spooling about the central axis of the particle (defined by extending the 12-fold axis of the portal to the coat pentamer on the opposite side of the particle), initially laying down a layer of coaxial rings adjacent to the protein capsid. This spool orientation is similar to that seen in T7 and epsilon 15 and so may be general, at least among the *Podoviridae* (*7*, *13*). It is impossible to discern from the structure, however, whether the first DNA rings deposited during packaging are adjacent to the portal or at the vertex opposite the portal. The structure is clearly a coaxial spool of DNA in contrast to concentric spool, "ball of twine" or folded DNA models. The icosahedrally averaged structure of P22 could not distinguish among these models, but the asymmetric reconstruction does.

Layers closest to the portal display the highest degree of order with individual rings of dsDNA clearly defined in the first and second layers when contoured at 2.5 times the standard deviation of the density (Fig. 3, B and C). At lower contour levels, five coaxial layers of DNA can be seen; the innermost is marginally discernible as a layer. Internal to this layer, the persistence length of the DNA cannot be accommodated in smooth rings, and more chaotic packing results. The DNA that occupies the central tube above the portal is most likely the last to enter during packaging, so that the vectorial injection of the DNA can proceed with the proper orientation (last base pairs in are the first base pairs out). No matter whether it is laid down first or last, the increasing disorder with distance from the portal suggests that it is the interaction with the portal that determines the overall orientation of the spool and arrangement of DNA within the virion. The exceptional order of the ring of DNA closest to the portal indicates that it is squeezed tightly against the portal in the infectious particle so that the portal pressure sensor is in the "on" position.

Our understanding of the P22 assembly pathway and the availability of a rich variety of mutant P22 particles, including those that lack ejection proteins or DNA, will allow further understanding of the structure described and definitive assignment of density to those gene products that are speculative at this time.

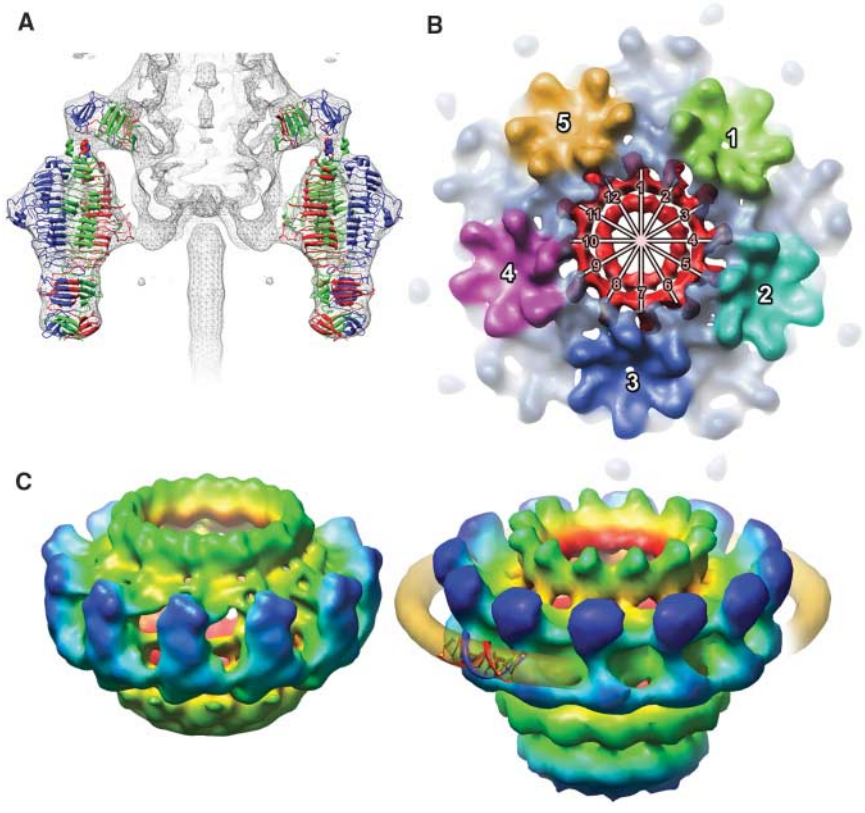

Fig. 4. P22 virion substructures. (**A**) Docking of tail-spike crystal structures. The crystal structure of the tail spike was solved as two separate parts, the virion-binding domain and the receptor-binding domain (*3*, *4*), and they fit into the six-fold averaged reconstruction density with exceptional accuracy. The reconstruction depicts the head-binding domain of the tail spike at an angle of 20° relative to the receptor-binding domain, indicating that there is a hinge between the two domains. This fitting also shows that the spike is in contact with gp4 and gp10 proteins in the tail tube at two distinct locations, one with the head-binding domain and a smaller one with the receptor-binding domain. (**B**) The coat-portal symmetry mismatch. The symmetry mismatch between the 12-fold portal (red) and the 5-fold opening in the $T = 7l$ coat protein surface lattice is shown with each hexamer of the capsid colored uniquely to emphasize the different units that form the 5-fold symmetric vertex. (**C**) Two P22 portal protein states. On the left is the 20 Å reconstruction of the free portal ring in solution (built from assembly of naïve gp1 subunits in vitro), and on the right is the portal ring that was virtually extracted from the asymmetric reconstruction of the P22 virion. The portal rings are colored radially such that density closest to the central axis is red, intermediate distance density is green, and the density farthest away is blue. Surrounding the intravirion portal is the first ring of dsDNA seen in the reconstruction (yellow) with a short segment of B-form dsDNA (PDB ID:1bna) arbitrarily docked into the density.

References and Notes

1. S. Casjens, P. Weigele, in *Viral Genome Packaging*, C. Catalano, Ed. (Landes Publishing, 2005), pp. 80–88.
2. P. E. Prevelige Jr., in *The Bacteriophages*, R. Calendar, Ed. (Oxford Univ. Press, New York, ed. 2, 2005), pp. 457–468.
3. S. Steinbacher *et al.*, *Proc. Natl. Acad. Sci. U.S.A.* **93**, 10584 (1996).
4. S. Steinbacher *et al.*, *J. Mol. Biol.* **267**, 865 (1997).
5. L. Tang, W. R. Marion, G. Cingolani, P. E. Prevelige, J. E. Johnson, *EMBO J.* **24**, 2087 (2005).
6. W. Jiang *et al.*, *Nat. Struct. Biol.* **10**, 131 (2003).
7. X. Agirrezabala *et al.*, *EMBO J.* **24**, 3820 (2005).
8. X. Agirrezabala *et al.*, *J. Mol. Biol.* **347**, 895 (2005).
9. A. Fokine *et al.*, *Proc. Natl. Acad. Sci. U.S.A.* **101**, 6003 (2004).
10. M. C. Morais *et al.*, *J. Struct. Biol.* **135**, 38 (2001).
11. Y. Tao *et al.*, *Cell* **95**, 431 (1998).
12. M. C. Morais *et al.*, *Mol. Cell* **18**, 149 (2005).

13. W. Jiang *et al.*, *Nature* **439**, 612 (2006).
14. S. Casjens, R. Hendrix, in *The Bacteriophages*, R. Calendar, Ed. (Plenum Press, New York, 1988), vol. 1, pp. 15–91.
15. A. A. Simpson *et al.*, *Nature* **408**, 745 (2000).
16. R. W. Hendrix, *Proc. Natl. Acad. Sci. U.S.A.* **75**, 4779 (1978).
17. S. Casjens *et al.*, *J. Mol. Biol.* **224**, 1055 (1992).
18. D. Anderson, S. Grimes, in *Viral Genome Packaging*, C. Catalano, Ed. (Landes Publishing, 2005), pp. 102–116.
19. S. Casjens, J. King, *J. Supramol. Struct.* **2**, 202 (1974).
20. D. Botstein, C. H. Waddell, J. King, *J. Mol. Biol.* **80**, 669 (1973).
21. J. King, E. V. Lenk, D. Botstein, *J. Mol. Biol.* **80**, 697 (1973).
22. V. Israel, *J. Virol.* **23**, 91 (1977).
23. B. Hoffman, M. Levine, *J. Virol.* **16**, 1547 (1975).
24. This work was supported by grants from the NIH and the NSF. The cryo-EM was conducted at the National Resource for Automated Molecular Microscopy, which is supported by the NIH through the National Center for Research Resources' P41 program (RR17573).

Supporting Online Material
www.sciencemag.org/cgi/content/full/1127981/DC1
Material and Methods
Figs. S1 to S4
References

28 March 2006; accepted 5 May 2006
Published online 18 May 2006;
10.1126/science.1127981
Include this information when citing this paper.

Metagenomic Analysis of Coastal RNA Virus Communities

Alexander I. Culley,[1] Andrew S. Lang,[2] Curtis A. Suttle[3]*

RNA viruses infect marine organisms from bacteria to whales, but RNA virus communities in the sea remain essentially unknown. Reverse-transcribed whole-genome shotgun sequencing was used to characterize the diversity of uncultivated marine RNA virus assemblages. A diverse assemblage of RNA viruses, including a broad group of marine picorna-like viruses, and distant relatives of viruses infecting arthropods and higher plants were found. Communities were dominated by distinct genotypes with small genome sizes, and we completely assembled the genomes of several hitherto undiscovered viruses. Our results show that the oceans are a reservoir of previously unknown RNA viruses.

High mutation rates and short generation times cause RNA viruses to exist as dynamic populations of genetic variants that are capable of using multiple host species (*1*). In the oceans, the largest ecosystem on Earth, RNA viruses infect ecologically and economically important organisms at all trophic levels, including heterotrophic bacteria (*2*), fish (*3*), crustaceans (*4*), and marine mammals (*5*). Recently, a series of previously unknown RNA viruses have been characterized that infect marine phytoplankton. These include positive-sense single-stranded (ss) RNA viruses (HaRNAV and HcRNAV) that lyse the toxic-bloom formers *Heterosigma akashiwo* and *Heterocapsa circularisquama* (*6*, *7*), a positive-sense ssRNA virus (RsRNAV) that infects the diatom *Rhizosolenia setigera* (*8*), and a double-stranded (ds) RNA virus (MpRNAV) with a genome organization similar to reoviruses that infects the cosmopolitan species *Micromonas pusilla* (*9*).

Despite the apparent importance of RNA viruses to marine organisms, almost nothing is known about natural communities of RNA viruses in the sea. The most tantalizing evidence that the diversity of RNA viruses in the sea extends well beyond what has been revealed in culture comes from a study that used gene-specific primers to target a subset of picorna-like viruses (*10*). The work showed that these positive-sense ssRNA viruses are persistent, widespread, and diverse members of marine virus communities.

Cultivation-independent genomic approaches have recently been used to characterize entire microbial (*11*, *12*) and bacteriophage (*13*, *14*) assemblages from a diversity of ecosystems. This approach does not require prior assumptions of the composition of the target community and produces data that can be used to estimate community structure. For this study we used randomly reverse-transcribed whole-genome shotgun sequencing to characterize the diversity of uncultivated marine RNA virus assemblages.

Natural virus communities were concentrated from English Bay at Jericho Pier (JP) and the Strait of Georgia (SOG), British Columbia, Canada (table S1). RNA was extracted from the purified virus fraction, reverse-transcribed into cDNA, and used to construct libraries representative of the natural RNA virus communities (*15*). Few sequence fragments [37 and 19% for JP and SOG, respectively (Fig. 1)] showed significant similarity [tBLASTx (*16*) expect value (E) < 0.001] to sequences in the National Center for Biotechnology Information (NCBI) database and no similarity to sequences from the Sargasso Sea microbial metagenome (*17*). In contrast, ~90% of Sargasso Sea microbial sequence fragments are notably similar to sequences in the NCBI database (*18*). These results imply that most RNA viruses in the sea are distantly related to known viruses and that their genetic diversity is much less explored relative to that of the prokaryotic community.

Sequence similarity (tBLASTx E < 0.001) in our samples revealed 98% of sequences belonged to positive-sense ssRNA viruses. The one exception was a sequence with similarity to a dsRNA virus. No RNA phage were detected, supporting arguments that most marine phages have DNA genomes (*19*) and that the predominate hosts of marine RNA viruses are eukaryotes. In addition, no sequences were similar to retroviral or negative-sense ssRNA viruses. Our results are minimum estimates of the richness of marine viral communities, because some viruses may have been excluded by our sam-

Table 1. Classification of significant tBLASTx matches (E value < 0.001, n = 92) to viral sequences into protein categories.

Protein classification	% of total viral hits
RNA-dependent RNA polymerase	39
Capsid	33
Unidentified structural	16
Unidentified nonstructural	7
Helicase	3
RNA binding protein	1
Replication initiator protein	1

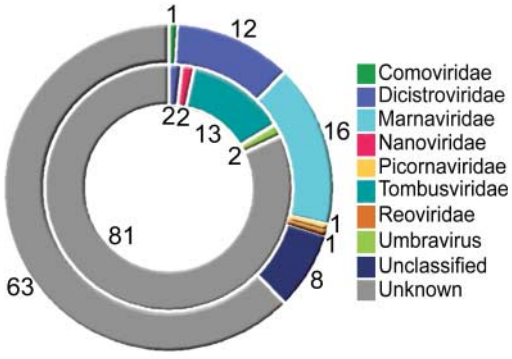

Fig. 1. Composition of the JP (outer circle, n = 216) and the SOG (inner circle, n = 61) libraries. The top tBLASTx matches of sequences from JP and SOG with the GenBank nonredundant database (E value < 0.001) are categorized by taxonomic group. Virus families or genera are color coded. The *Comoviridae*, *Dicistroviridae*, *Marnaviridae*, and *Picornaviridae* are families in the proposed order *Picornavirales* (*25*). The percent values for each virus group in each library are shown. The identification of the individual viruses from each taxonomic group can be found in table S1.

[1]Department of Botany, University of British Columbia, 3529-6270 University Boulevard, Vancouver, BC V6T 1Z4, Canada. [2]Institute of Marine Science, University of Alaska Fairbanks, 905 North Koyukuk Drive, Fairbanks, AK 99775, USA. [3]Department of Earth and Ocean Sciences, Department of Microbiology and Immunology, Department of Botany, University of British Columbia, 1461-6270 University Boulevard, Vancouver, BC V6T 1Z4, Canada.

*To whom correspondence should be addressed. E-mail: csuttle@eos.ubc.ca